CANADIAN APPLIED
MATHEMATICS QUARTERLY
Volume 16, Number 4, Winter 2008

CALCULATION OF POTENTIAL FLOW AROUND AN OBLATE SPHEROID USING A BOUNDARY ELEMENT METHOD

G. MUHAMMAD,[1] N. A. SHAH,[2] M. MUSHTAQ[3]
AND S. AHMAD[3]

ABSTRACT. In this paper a direct boundary element method is applied to calculate an incompressible potential flow around an oblate spheroid. The computed results for flow velocities are compared with analytical results. The accuracy of the computed results is quite good.

1 Flow past an oblate spheroid Let an oblate spheroid be generated by rotating an ellipse of semi-major axis a and semi-minor axis b about its minor axis and let a uniform stream of velocity U be in the positive direction of the z-axis as shown in Figure 1. An axisymmetric

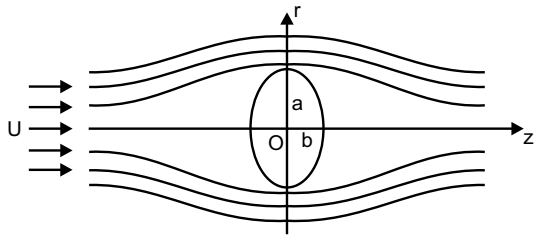

FIGURE 1

flow is most conveniently formulated in cylindrical polar coordinates. The cylindrical polar coordinates are taken as (r, θ, z).

[1]PhD Scholar, Department of Mathematics, U. E. T. Lahore, Pakistan.
[2]Meritorious Professor, Department of Mathematics, U. E. T. Lahore, Pakistan.
[3]Department of Mathematics, U. E. T. Lahore, Pakistan.

The oblate spheriod is defined by the transformation

$$\begin{aligned} z + ir &= c\sinh\zeta \\ &= c\sinh(\xi + i\eta) \\ &= c(\sinh\xi\cos\eta + i\cosh\xi\sin\eta) \\ &= c\sinh\xi\cos\eta + ic\cosh\xi\sin\eta. \end{aligned}$$

Comparing real and imaginary parts, we have

$$z = c\sinh\xi\cos\eta \qquad \text{and} \qquad r = c\cosh\xi\sin\eta, \tag{1.1}$$

which are for an oblate spheroid. Therefore, the curve $\xi = \xi_0$ is an ellipse in the zr-plane whose semi-axes are

$$a = c\cosh\xi_0 \qquad \text{and} \qquad b = c\sinh\xi_0, \tag{1.2}$$

and so $\xi = \xi_0$ is an oblate spheroid.

The stream function Ψ for an oblate spheroid moving in the negative z-direction with velcity U can be calculated as

$$\Psi = \frac{\frac{1}{2}Uc^2\left[\sinh\xi - \cosh^2\xi\cot^{-1}(\sinh\xi)\right]\sin^2\eta}{e\sqrt{1-e^2} - \sin^{-1}e}, \tag{1.3}$$

where e is the eccentricity.

Also the stream function Ψ for the uniform stream with velocity U in the positive z-direction is given by

$$\Psi = -\frac{1}{2}Ur^2. \tag{1.4}$$

Therefore, the stream function Ψ for the streaming motion past a fixed oblate spheroid in the positive z-direction becomes

$$\Psi = -\frac{1}{2}Ur^2 + \frac{\frac{1}{2}Uc^2\left[\sinh\xi - \cosh^2\xi\cot^{-1}(\sinh\xi)\right]\sin^2\eta}{e\sqrt{1-e^2} - \sin^{-1}e},$$

which on using (1.1) becomes

$$\begin{aligned} \Psi = &-\frac{1}{2}Uc^2\cosh^2\xi\sin^2\eta \\ &+ \frac{\frac{1}{2}Uc^2\left[\sinh\xi - \cosh^2\xi\cot^{-1}(\sinh\xi)\right]\sin^2\eta}{e\sqrt{1-e^2} - \sin^{-1}e}. \end{aligned} \tag{1.5}$$

In order to determine the formula for the velocity, the following relation is used

$$V^2 r^2 f'(\zeta)\overline{f'}\left(\overline{\zeta}\right) = \left(\frac{\partial \Psi}{\partial \xi}\right)^2 + \left(\frac{\partial \Psi}{\partial \eta}\right)^2, \tag{1.6}$$

where $f(\zeta) = c\sinh\zeta$, and therefore

$$f'(\zeta) = c\cosh\zeta = c\cosh(\xi + i\eta) \qquad \text{and} \qquad \overline{f'}\left(\overline{\zeta}\right) = c\cosh(\xi - i\eta),$$

so that

$$f'(\zeta)\,\overline{f'}\left(\overline{\zeta}\right) = c^2\left(\cosh^2\xi\cos^2\eta + \sinh^2\xi\sin^2\eta\right). \tag{1.7}$$

When $\xi = \xi_0$, then from (1.1), (1.6), and (1.7) we have

$$V^2 c^4 \cosh^2\xi_0 \sin^2\eta\left(\cosh^2\xi_0\cos^2\eta + \sinh^2\xi_0\sin^2\eta\right) = \left(\frac{\partial \Psi}{\partial \xi}\right)^2_{\xi=\xi_0} + \left(\frac{\partial \Psi}{\partial \eta}\right)^2_{\xi=\xi_0}. \tag{1.8}$$

Now, from (1.5) we get

$$\left(\frac{\partial \Psi}{\partial \xi}\right)_{\xi=\xi_0} = -Uc^2\cosh\xi_0\sinh\xi_0\sin^2\eta + \frac{Uc^2\left[\cosh\xi_0 - \cosh\xi_0\sinh\xi_0\cot^{-1}\left(\sinh\xi_0\right)\right]\sin^2\eta}{e\sqrt{1-e^2} - \sin^{-1}e}. \tag{1.9}$$

Since for an oblate spheroid we have

$$a = c\cosh\xi_0 \qquad \text{and} \qquad b = c\sinh\xi_0, \tag{1.10}$$

but

$$\cot^{-1}\left(\sinh\xi_0\right) = \theta \qquad \text{and} \qquad e = \sin\theta = \frac{c}{a},$$

and so

$$\sqrt{1-e^2} = \cos\theta = \frac{b}{a}. \tag{1.11}$$

From (1.9), (1.10), and (1.11), we get

$$\left(\frac{\partial \Psi}{\partial \xi}\right)_{\xi=\xi_0} = U\sin^2\eta\left\{-ab+\frac{ac-ab\theta}{\frac{c}{a}\cdot\frac{b}{a}-\theta}\right\} \tag{1.12}$$

$$= U\sin^2\eta\left\{-ab+\frac{ac-ab\theta}{bc-a^2\theta}\,a^2\right\}$$

And from (1.5), (1.10), and (1.11), we obtain

$$\left(\frac{\partial \Psi}{\partial \eta}\right)_{\xi=\xi_0} = 0 \tag{1.13}$$

Using (1.12) and (1.13), (1.8) becomes

$$V^2c^4\cosh^2\xi_0\sin^2\eta\left(\cosh^2\xi_0\cos^2\eta+\sinh^2\xi_0\sin^2\eta\right) \tag{1.14}$$

$$= U^2\sin^4\eta\left[-ab+\frac{ac-ab\theta}{bc-a^2\theta}\,a^2\right]^2,$$

but from (1.1) and (1.2) we get

$$\cos\eta = \frac{z}{b} \qquad \text{and} \qquad \sin\eta = \frac{r}{a}. \tag{1.15}$$

Using (1.10) and (1.15) in (1.14), we have

$$V^2 = \frac{U^2r^2b^2c^6}{(bc-a^2\theta)^2(a^4z^2+b^4r^2)} \tag{1.16}$$

where $\theta = \sin^{-1}(c/a)$.

Taking the square root of the expression in (1.16), the magnitude of the exact velocity distribution over the boundary of an oblate spheroid is given by

$$V = \frac{Ubc^3r}{(bc-a^2\theta)\sqrt{a^4z^2+b^4r^2}}.$$

2 Boundary conditions The boundary condition to be satisfied over the surface of an oblate spheroid is

$$\frac{\partial \phi_{o.s}}{\partial n} = U\left(\widehat{n}\cdot\widehat{k}\right) \tag{2.1}$$

where $\phi_{o.s}$ is the perturbation velocity potential of an oblate spheroid and $\widehat{n}$ is the outward drawn normal to the surface of an oblate spheroid.

If the equation of the boundary of the oblate spheroid is

$$\frac{z^2}{b^2}+\frac{y^2}{a^2}+\frac{x^2}{a^2}=1,$$

and we let

$$f(x,y,z)=\frac{z^2}{b^2}+\frac{y^2}{a^2}+\frac{x^2}{a^2}-1,$$

then

$$\nabla f=\frac{2x}{a^2}\,\widehat{i}+\frac{2y}{a^2}\,\widehat{j}+\frac{2z}{b^2}\,\widehat{k}.$$

and therefore

$$\widehat{n}=\frac{\nabla f}{\|\nabla f\|}=\frac{\dfrac{2x}{a^2}\,\widehat{i}+\dfrac{2y}{a^2}\,\widehat{j}+\dfrac{2z}{b^2}\,\widehat{k}}{\sqrt{\left(\dfrac{2z}{b^2}\right)^2+\left(\dfrac{2y}{a^2}\right)^2+\left(\dfrac{2x}{a^2}\right)^2}}$$

Thus,

$$\widehat{n}\cdot\widehat{k}=\frac{\dfrac{2z}{b^2}}{\sqrt{\left(\dfrac{2z}{b^2}\right)^2+\left(\dfrac{2y}{a^2}\right)^2+\left(\dfrac{2x}{a^2}\right)^2}}$$

$$=\frac{\dfrac{z}{b^2}}{\sqrt{\dfrac{z^2}{b^4}+\dfrac{y^2}{a^4}+\dfrac{x^2}{a^4}}}.$$

Therefore, the boundary condition (2.1) takes the form

$$\frac{\partial\phi_{o.s}}{\partial n}=U\,\frac{\dfrac{z}{b^2}}{\dfrac{\sqrt{a^2z^2+b^4y^2+b^2x^2}}{a^2b^2}}$$

$$=\frac{za^2}{\sqrt{a^4z^2+b^4(y^2+x^2)}}\qquad(\text{taking}\quad U=1).\tag{2.2}$$

Equation (2.2) is the boundary condition which must be satisfied over the boundary of an oblate spheroid.

3 Process of discretization A direct boundary element method is appled to calculate the potential flow solution around the oblate spheroid for which the analytical solution is available.

Consider the surface of the sphere in one octant to be divided into three quadrilateral elements by joining the centroid of the surface with the midpoints of the curves in the coordinate planes as shown in Figure 2. Then each element is divided futher into four elements by joining the

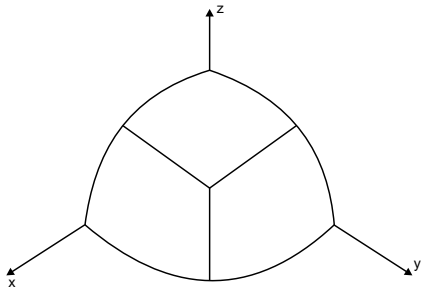

FIGURE 2

centroid of that element with the midpoint of each side of the element. Thus one octant of the surface of the sphere is divided into 12 elements and the whole surface of the body is divided into 96 boundary elements. The above mentioned method is adopted in order to produce a uniform distribution of elements over the surface of the body.

Figure 3 shows the method for finding the coordinates (x_p, y_p, z_p) of any point P on the surface of the sphere.

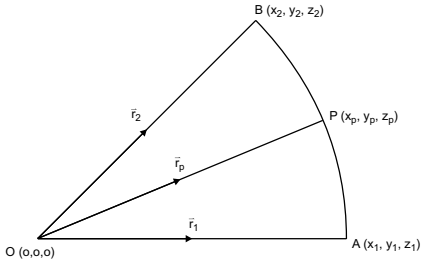

FIGURE 3

From Figure 3 we have the following equations

$$\|\overrightarrow{r_p}\| = 1, \quad \overrightarrow{r_p} \cdot \overrightarrow{r_1} = \overrightarrow{r_p} \cdot \overrightarrow{r_2}, \quad (\overrightarrow{r_1} - \overrightarrow{r_2}) \cdot \overrightarrow{r_p} = 0,$$

or in Cartesian form,

$$\begin{aligned} &x_p^2 + y_p^2 + z_p^2 = 1 \\ &x_p(x_1 - x_2) + y_p(y_1 - y_2) + z_p(z_1 - z_2) = 0 \\ &x_p(y_1 z_2 - z_1 y_2) + y_p(x_2 z_1 - x_1 z_2) + z_p(x_1 y_2 - x_2 y_1) = 0. \end{aligned}$$

As the body possesses planes of symmetry, this fact may be used in the input to the program and only the nonredundant portion need be specified by input points. The other points are automatically taken into account. The planes of symmetry are taken to be the coordinate planes of the reference coordinate system. The advantage of the use of symmetry is that it reduces the order of the resulting system of equations and consequently reduces the computing time in running a program. As a sphere is symmetric with respect to all three coordinate planes of the reference coordinate system, only one eighth of the body surface need be specified by the input points, while the other seven eighths can be accounted for by symmetry.

The oblate spheroids of fineness ratios 2 and 10 are discretised into 24 and 96 boundary elements and the computed velocity distributions are compared with analytical solutions for the oblate spheroids. In both cases of spheroids, the input points are distributed on the surface of a sphere and the x- and y-coordinates of these points are then divided by the fineness ratios to generate the points for the oblate spheroids. The number of boundary elements used to obtain the computed velocity distribution are the same as are used for the sphere.

The calculated velocity distributions are compared with analytical solutions for the oblate spheroid of fineness ratios 2 and 10 using Fortran programming.

Table 1 shows the comparison of the computed velocities with exact velocities over the surface of an ablate spheroid with fineness ratio 2 using 24 boundary elements.

Table 2 shows the comparison of the computed velocities with exact velocities over the surface of an oblate spheroid with fineness ratio 10 using 24 elements.

TABLE 1

Element	XM	YM	ZM	$R = \sqrt{(\text{YM})^2 + (\text{ZM})^2}$	Computed Velocity	Exact Velocity
1	−.161E + 00	−.748E + 00	.321E + 00	.814E + 00	.13949E + 01	.16604E + 01
2	−.374E + 00	−.321E + 00	.321E + 00	.454E + 00	.48364E + 00	.61445E + 00
3	−.374E + 00	.321E + 00	.321E + 00	.454E + 00	.48364E + 00	.61445E + 00
4	−.161E + 00	.748E + 00	.321E + 00	.814E + 00	.13949E + 01	.16604E + 01
5	.161E + 00	.748E + 00	.321E + 00	.814E + 00	.13949E + 01	.16604E + 01
6	.374E + 00	.321E + 00	.321E + 00	.454E + 00	.48364E + 00	.61445E + 00
7	.374E + 00	−.321E + 00	.321E + 00	.454E + 00	.48364E + 00	.61445E + 00
8	.161E + 00	.748E + 00	.321E + 00	.814E + 00	.13949E + 01	.16604E + 01
9	−.161E + 00	−.312E + 00	.748E + 00	.814E + 00	.13949E + 01	.16604E + 01
10	−.161E + 00	.312E + 00	.748E + 00	.814E + 00	.13949E + 01	.16604E + 01
11	.161E + 00	.312E + 00	.748E + 00	.814E + 00	.13949E + 01	.16604E + 01
12	.161E + 00	−.312E + 00	.748E + 00	.814E + 00	.13949E + 01	.16604E + 01

TABLE 2

Element	XM	YM	ZM	$R = \sqrt{(\text{YM})^2 + (\text{ZM})^2}$	Computed Velocity	Exact Velocity
1	−.321E − 01	−.748E + 00	.321E + 00	.814E + 00	.82669E + 00	.17651E + 01
2	−.748E − 01	−.321E + 00	.321E + 00	.454E + 00	.31052E + 00	.43542E + 00
3	−.748E − 01	.321E + 00	.321E + 00	.454E + 00	.31052E + 00	.43542E + 00
4	−.321E − 01	.748E + 00	.321E + 00	.814E + 00	.82669E + 00	.17651E + 01
5	.321E − 01	.748E + 00	.321E + 00	.814E + 00	.82669E + 00	.17651E + 01
6	.748E − 01	.321E + 00	.321E + 00	.454E + 00	.31052E + 00	.43542E + 00
7	.748E − 01	−.321E + 00	.321E + 00	.454E + 00	.31052E + 00	.43542E + 00
8	.321E − 01	−.748E + 00	.321E + 00	.814E + 00	.82669E + 00	.17651E + 01
9	−.321E − 01	−.312E + 00	.748E + 00	.814E + 00	.82669E + 00	.17651E + 01
10	−.321E − 01	.312E + 00	.748E + 00	.814E + 00	.82669E + 00	.17651E + 01
11	.321E − 01	.312E + 00	.748E + 00	.814E + 00	.82669E + 00	.17651E + 01
12	.321E − 01	.312E + 00	.748E + 00	.814E + 00	.82669E + 00	.17651E + 01

Table 3 shows the comparison of the computed velocities with exact velocities over the surface of an oblate shperoid with fineness ratio 2 using 96 boundary elements.

TABLE 3

Element	XM	YM	ZM	$R = \sqrt{(\text{YM})^2 + (\text{ZM})^2}$	Computed Velocity	Exact Velocity
1	−.885E − 01	−.935E + 00	.177E + 00	.951E + 00	.17954E + 01	.19822E + 01
2	−.261E + 00	−.798E + 00	.157E + 00	.814E + 00	.12657E + 01	.12998E + 01
3	−.399E + 00	−.522E + 00	.157E + 00	.545E + 00	.67432E + 00	.68362E + 00
4	−.467E + 00	−.177E + 00	.177E + 00	.250E + 00	.25026E + 00	.28082E + 00
5	−.467E + 00	.177E + 00	.177E + 00	.250E + 00	.25026E + 00	.28082E + 00
6	−.399E + 00	.522E + 00	.157E + 00	.545E + 00	.67432E + 00	.68362E + 00
7	−.261E + 00	.798E + 00	.157E + 00	.814E + 00	.12657E + 01	.12998E + 01
8	−.885E − 01	.935E + 00	.177E + 00	.951E + 00	.17954E + 01	.19822E + 01
9	.885E − 01	.935E + 00	.177E + 00	.951E + 00	.17954E + 01	.19822E + 01
10	.261E + 00	.798E + 00	.157E + 00	.814E + 00	.12657E + 01	.12998E + 01
11	.399E + 00	.522E + 00	.157E + 00	.545E + 00	.67432E + 00	.68362E + 00
12	.467E + 00	.177E + 00	.177E + 00	.250E + 00	.25026E + 00	.28082E + 00
13	.467E + 00	−.177E + 00	.177E + 00	.250E + 00	.25026E + 00	.28082E + 00
14	.399E + 00	−.522E + 00	.157E + 00	.545E + 00	.67432E + 00	.68362E + 00
15	.261E + 00	−.798E + 00	.157E + 00	.814E + 00	.12657E + 01	.12998E + 01
16	.885E − 01	−.935E + 00	.177E + 00	.951E + 00	.17954E + 01	.19822E + 01
17	−.785E − 01	−.798E + 00	.522E + 00	.954E + 00	.17828E + 01	.20090E + 01
18	−.235E + 00	−.703E + 00	.470E + 00	.846E + 00	.14249E + 01	.14150E + 01
19	−.352E + 00	−.470E + 00	.470E + 00	.664E + 00	.80589E + 00	.90333E + 00
20	−.399E + 00	−.157E + 00	.522E + 00	.545E + 00	.67432E + 00	.68362E + 00
21	−.399E + 00	.157E + 00	.522E + 00	.545E + 00	.67432E + 00	.68362E + 00
22	−.352E + 00	.470E + 00	.470E + 00	.664E + 00	.80589E + 00	.90333E + 00
23	−.235E + 00	.703E + 00	.470E + 00	.846E + 00	.14249E + 01	.14150E + 01
24	−.785E − 01	.798E + 00	.522E + 00	.954E + 00	.17828E + 01	.20090E + 01
25	.785E − 01	.798E + 00	.522E + 00	.954E + 00	.17828E + 01	.20090E + 01
26	.235E + 00	.703E + 00	.470E + 00	.846E + 00	.14249E + 01	.14150E + 01
27	.352E + 00	.470E + 00	.470E + 00	.664E + 00	.80589E + 00	.90333E + 00
28	.399E + 00	.157E + 00	.522E + 00	.545E + 00	.67432E + 00	.68362E + 00
29	.399E + 00	−.157E + 00	.522E + 00	.545E + 00	.67432E + 00	.68362E + 00
30	.352E + 00	−.470E + 00	.470E + 00	.664E + 00	.80589E + 00	.90333E + 00
31	.235E + 00	−.703E + 00	.470E + 00	.846E + 00	.14249E + 01	.14150E + 01
32	.785E − 01	−.798E + 00	.522E + 00	.954E + 00	.17828E + 01	.20090E + 01
33	−.785E − 01	−.522E + 00	.798E + 00	.954E + 00	.17828E + 01	.20090E + 01
34	−.235E + 00	−.470E + 00	.703E + 00	.846E + 00	.14249E + 01	.14150E + 01
35	−.261E + 00	−.157E + 00	.798E + 00	.814E + 00	.12657E + 01	.12998E + 00

36	−.261E + 00	.157E + 00	.798E + 00	.814E + 00	.12657E + 01	.12998E + 00
37	−.235E + 00	.470E + 00	.703E + 00	.846E + 00	.14249E + 01	.14150E + 01
38	−.785E − 01	.522E + 00	.798E + 00	.954E + 00	.17828E + 01	.20090E + 01
39	.785E − 01	.522E + 00	.798E + 00	.954E + 00	.17828E + 01	.20090E + 01
40	.235E + 00	.470E + 00	.703E + 00	.846E + 00	.14249E + 01	.14150E + 01
41	.261E + 00	.157E + 00	.798E + 00	.814E + 00	.12657E + 01	.12998E + 00
42	.261E + 00	−.157E + 00	.798E + 00	.814E + 00	.12657E + 01	.12998E + 00
43	.235E + 00	−.470E + 00	.703E + 00	.846E + 00	.14249E + 01	.14150E + 01
44	.785E − 01	−.522E + 00	.798E + 00	.954E + 00	.17828E + 01	.20090E + 01
45	−.885E − 01	−.177E + 00	.934E + 00	.951E + 00	.17954E + 01	.19822E + 01
46	−.885E − 01	.177E + 00	.934E + 00	.951E + 00	.17954E + 01	.19822E + 01
47	.885E − 01	.177E + 00	.934E + 00	.951E + 00	.17954E + 01	.19822E + 01
48	.885E − 01	−.177E + 00	.934E + 00	.951E + 00	.17954E + 01	.19822E + 01

Table 4 shows the comparison of the computed velocities with exact velocities over the surface of an oblate spheroid with fineness ratio 10 using 96 boundary elements.

TABLE 4

Element	XM	YM	ZM	$R = \sqrt{(\mathrm{YM})^2 + (\mathrm{ZM})^2}$	Computed Velocity	Exact Velocity
1	−.177E − 01	−.934E + 00	.177E + 00	.951E + 00	.20069E + 01	.34000E + 01
2	−.522E − 01	−.798E + 00	.157E + 00	.814E + 00	.13142E + 01	.11059E + 01
3	−.798E − 01	−.522E + 00	.157E + 00	.545E + 00	.52593E + 00	.48960E + 00
4	−.934E − 01	−.177E + 00	.177E + 00	.250E + 00	.18238E + 00	.19241E + 00
5	−.934E − 01	.177E + 00	.177E + 00	.250E + 00	.18238E + 00	.19241E + 00
6	−.798E − 01	.522E + 00	.157E + 00	.545E + 00	.52593E + 00	.48960E + 00
7	−.522E − 01	.798E + 00	.157E + 00	.814E + 00	.13142E + 01	.11059E + 01
8	−.177E − 01	.934E + 00	.177E + 00	.951E + 00	.20069E + 01	.34000E + 01
9	.177E − 01	.934E + 00	.177E + 00	.951E + 00	.20069E + 01	.34000E + 01
10	.522E − 01	.798E + 00	.157E + 00	.814E + 00	.13142E + 01	.11059E + 01
11	.798E − 01	−.522E + 00	.157E + 00	.545E + 00	.52593E + 00	.48960E + 00
12	.934E − 01	.177E + 00	.177E + 00	.250E + 00	.18238E + 00	.19241E + 00
13	.934E − 01	−.177E + 00	.177E + 00	.250E + 00	.18238E + 00	.19241E + 00
14	.798E − 01	−.522E + 00	.157E + 00	.545E + 00	.52593E + 00	.48960E + 00
15	.522E − 01	−.798E + 00	.157E + 00	.814E + 00	.13142E + 01	.11059E + 01
16	.177E − 01	−.934E + 00	.177E + 00	.951E + 00	.20069E + 01	.34000E + 01
17	−.157E − 01	−.798E + 00	.522E + 00	.954E + 00	.17718E + 01	.37304E + 01
18	−.470E − 01	−.703E + 00	.470E + 00	.846E + 00	.16573E + 01	.12729E + 01

19	−.703E − 01	−.470E + 00	.470E + 00	.664E + 00	.62015E + 00	.67567E + 00
20	−.798E − 01	−.157E + 00	.522E + 00	.545E + 00	.52593E + 00	.48960E + 00
21	−.798E − 01	.157E + 00	.522E + 00	.545E + 00	.52593E + 00	.48960E + 00
22	−.703E − 01	.470E + 00	.470E + 00	.664E + 00	.62015E + 00	.67567E + 00
23	−.470E − 01	.703E + 00	.470E + 00	.846E + 00	.16573E + 01	.12729E + 01
24	−.157E − 01	.798E + 00	.522E + 00	.954E + 00	.17718E + 01	.37304E + 01
25	.157E − 01	.798E + 00	.522E + 00	.954E + 00	.17718E + 01	.37304E + 01
26	.470E − 01	.703E + 00	.470E + 00	.846E + 00	.16573E + 01	.12729E + 01
27	.703E − 01	.470E + 00	.470E + 00	.664E + 00	.62015E + 00	.67567E + 00
28	.798E − 01	.157E + 00	.522E + 00	.545E + 00	.52593E + 00	.48960E + 00
29	.798E − 01	−.157E + 00	.522E + 00	.545E + 00	.52593E + 00	.48960E + 00
30	.703E − 01	−.470E + 00	.470E + 00	.664E + 00	.62015E + 00	.67567E + 00
31	.470E − 01	−.703E + 00	.470E + 00	.846E + 00	.16573E + 01	.12729E + 01
32	.157E − 01	−.798E + 00	.522E + 00	.954E + 00	.17718E + 01	.37304E + 01
33	−.157E − 01	−.522E + 00	.798E + 00	.954E + 00	.17718E + 01	.37304E + 01
34	−.470E − 01	−.470E + 00	.703E + 00	.846E + 00	.16573E + 01	.12729E + 01
35	−.522E − 01	−.157E + 00	.798E + 00	.814E + 00	.13142E + 01	.11059E + 01
36	−.522E − 01	.157E + 00	.798E + 00	.814E + 00	.13142E + 01	.11059E + 01
37	−.470E − 01	.470E + 00	.703E + 00	.846E + 00	.16573E + 01	.12729E + 01
38	−.157E − 01	.522E + 00	.798E + 00	.954E + 00	.17718E + 01	.37304E + 01
39	.157E − 01	.522E + 00	.798E + 00	.954E + 00	.17718E + 01	.37304E + 01
40	.470E − 01	.470E + 00	.703E + 00	.846E + 00	.16573E + 01	.12729E + 01
41	.522E − 01	.157E + 00	.798E + 00	.814E + 00	.13142E + 01	.11059E + 01
42	.522E − 01	−.157E + 00	.798E + 00	.814E + 00	.13142E + 01	.11059E + 01
43	.470E − 01	−.470E + 00	.703E + 00	.846E + 00	.16573E + 01	.12729E + 01
44	.157E − 01	−.522E + 00	.798E + 00	.954E + 00	.17718E + 01	.37304E + 01
45	−.177E − 01	−.177E + 00	.934E + 00	.951E + 00	.20068E + 01	.34000E + 01
46	−.177E − 01	.177E + 00	.934E + 00	.951E + 00	.20068E + 01	.34000E + 01
47	.177E − 01	.177E + 00	.934E + 00	.951E + 00	.20068E + 01	.34000E + 01
48	.177E − 01	−.177E + 00	.934E + 00	.951E + 00	.20068E + 01	.34000E + 01

Figures 4 and 6 show the comparison of the computed and analytical distributions over the surface of an oblate spheroid of fineness ratio 2 for 24 and 96 boundary elements, respectively. Figures 5 and 7 show the comparison of the computed and analytical distributions over the surface of an oblate spheroid of fineness ratio 10 for 24 and 96 boundary elements, respectively.

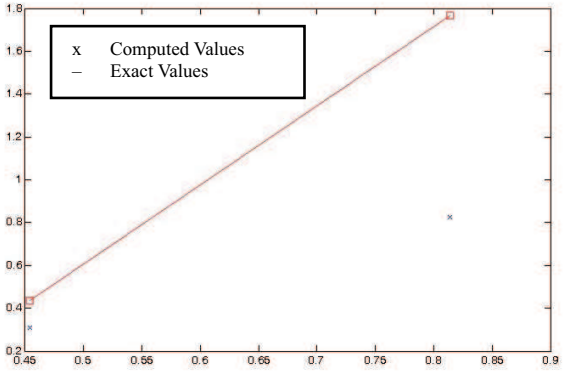

FIGURE 4: Comparison of computed and analytical velocity distributions over the surface of an oblate spheroid using 24 boundary elements with fineness ratio 2.

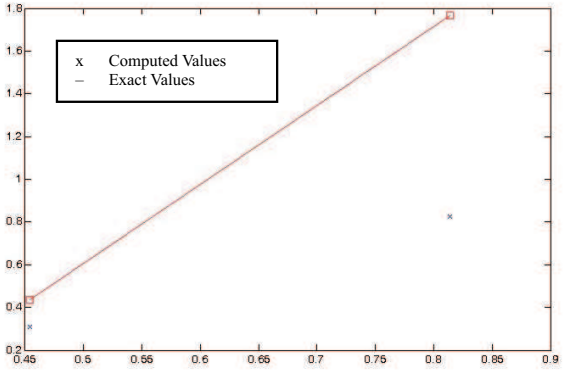

FIGURE 5: Comparison of computed and analytical velocity distributions over the surface of an oblate spheroid using 24 boundary elements with fineness ratio 10.

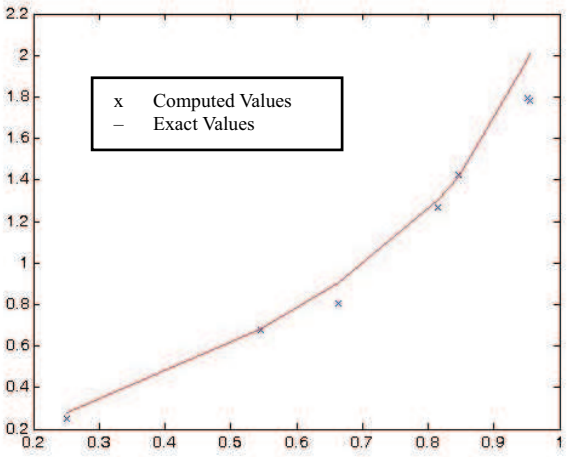

FIGURE 6: Comparison of computed and analytical velocity distributions over the surface of an oblate spheroid using 96 boundary elements with fineness ratio 2.

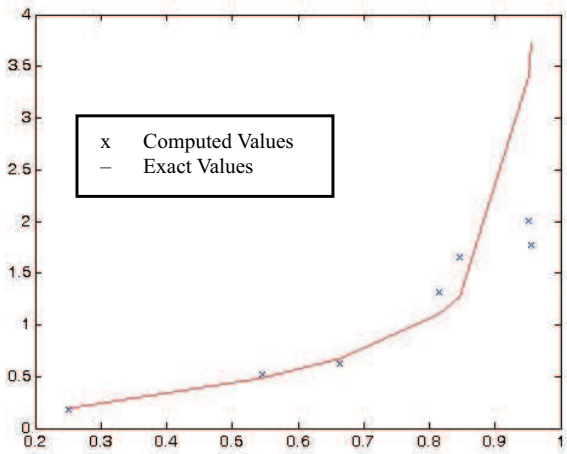

FIGURE 7: Comparison of computed and analytical velocity distributions over the surface of an oblate spheroid using 96 boundary elements with fineness ratio 10.

4 Conclusion A direct boundary element method is applied for calculation of an incompressible potential flow around an oblate spheroid. The computed flow velocities obtrained by this method are compared with the analytical solutions for flow past an oblate spheroid. It is found that the computed results for velocity distribution are in good agreement with the analytical results for the body under consideration.

Acknowledgement We are thankful to the University of Engineering & Technology, Lahore-Pakistan, for financial support.

REFERENCES

1. C. A. Brebbia, *The Boundary Element Method for Engineers*, Pentech Press, 1978.
2. C. A. Brebbia and S. Walker, *Boundary Element Techniques in Engineering*, Newnes-Butterworths, 1980.
3. J. L. Hess and A. M. O. Smith, *Calculation of potential flow about arbitrary bodies*, Progr. Aeronautical Sci. **8** (1967), 1–158.
4. J. L. Hess, *Higher order numerical solutions of the integral equation for the two-dimensional Neumann problem*, Comput. Methods Appl. Mech. Engrg. **2** (1973), 1–15.
5. L. M. Milne-Thomson, *Theoretical Hydrodynamics*, 5th Edition, Macmillan & Co. Ltd, London, 1968.
6. L. Morino, Lee-Tzong Chen and E.O. Suciu, *A steady and oscillatory subsonic and supersonic aerodunamics around complex configuration*, AIAA J. **13**(3), (1975), 368–374.
7. M. Mushtaq, N. A. Shah, G. Muhammad and G. Z. Rizve, *Calculation of potential flow around an oblate spheroid using indirect boundary element method,* Kasetsart J. Natural Sci. **43**(4) (2009).
8. Basri Nor Shah *et al*, *Incompressible Potential Flow Analysis Using Panel Method*, Universiti Purta, Malaysia, 2005.
9. N. A. Shah, *Ideal Fluid Dynamics,* A-one publishers, Lahore-Pakistan, 553–561, 2008.

Corresponding author: M. Mushtaq
Department of Mathematics, University of Engineering & Technology, Lahore-Pakistan
E-mail address: mushtaqmalik2004@yahoo.co.uk

G. Muhammad, N. A. Shah, S. Ahmad
Department of Mathematics, University of Engineering & Technology, Lahore-Pakistan